

# Controlled phase gate in exchange coupled quantum dots affected by quasistatic charge noise

Yinan Fang<sup>1,2\*</sup>

<sup>1</sup>*School of Physics and Astronomy and Yunnan Key Laboratory for Quantum Information, Yunnan University, Kunming 650500, China*

<sup>2</sup>*Beijing Computational Science Research Center, Beijing 100193, People's Republic of China*

Charge noise has been one of the main issues in realizing high fidelity two-qubit quantum gates in semiconductor based qubits. Here, we study the influence of quasistatic noise in quantum dot detuning on the controlled phase gate for spin qubits that defined on a double quantum dot. Analytical expressions for the noise averaged Hamiltonian, exchange interaction, as well as the gate fidelity are derived for weak noise covering experimental relevant regime. We also perform interleaved two-qubit randomized benchmarking analysis for the controlled phase gate and show that an exponential decay of the sequential fidelity is still valid for the weak noise.

## I. INTRODUCTION

Implementing high fidelity gates driven by the pursuit for a large scale quantum computational device had been witnessed with remarkable progresses during the past decades. In spin qubits based on the semiconductor quantum dot (QD) [1, 2], single as well as two qubits gates fidelity exceeding or close to the threshold of quantum error correction on the surface code [3–5] had been routinely achieved [6–8]. Meanwhile, architectures for a scalable design were proposed for spin qubits that based on the phosphorus donor [9] and QDs [10–12]. Recently, coherent control and spin readout were demonstrated for a three-by-three two-dimensional QD array in GaAs/AlGaAs [13], and devices operated at a higher temperature enabling larger cooling power were also realized in isotopically purified silicon [14].

In contrast to single qubit gates usually implemented by applying with an oscillating magnetic field, a natural way to implement the two-qubit operation in gate defined in a double quantum dot (DQD) is to utilize the Heisenberg exchange interaction  $J$  [1, 15, 16]. Usually, electric noise affects  $J$  in DQD more strongly than those parameters that involved in single qubit gates, as it depends significantly on the confining potential and the overlap of the electron wave functions [15, 17]. Furthermore, the suppression of magnetic noise using techniques such as dynamical decoupling and isotopically purification makes the charge noise the current bottleneck in order to reach threshold fidelity for two-qubit gates error correction [7]. Also the readout fidelity was shown to be limited by electric noise [18]. Therefore, a better understanding on the decoherence effect of charge noise accounting for the state-of-art progress in QD based spin qubits would be beneficial in further boosting the two-qubit gate fidelities towards the ultimate goal of quantum error correction.

The source of charge noise could either be mobile or fixed [19]. One typical example of mobile charge noise is

due to fluctuating two-level systems near the QDs, while the fixed charge noise is due to static disorders. In this regards, a usually employed approach to study the detrimental effect of charge noise in QD is to assume that the noise affects the system only quasistatically, where the typical frequency of the noise is smaller than  $1/T_2^*$  [20]. Under such assumption,  $J$  is taken as a fixed quantity during each implementation of a quantum gate but can vary randomly between successive execute of the gate, then physical quantities are calculated by average over the distribution of  $J$ . The quasistatic model of charge noise had been applied in the calculation of the electron spin inhomogeneous dephasing time  $T_2^*$  [21–24], and it reveals effects such as the transition from power-law to exponential decay in free induced decay signals [20, 23].

In this work, we investigate theoretically the influence of charge noise on the controlled phase (CPHASE) gate in a DQD. Instead of imposing phenomenological noise distributions on  $J$ , we rely on a microscopic model which accounts for the dependence of  $J$  on these parameters that are directly connected to charge fluctuations [23]. Perturbative results on the experimental relevant quantities such as the spin-up fraction and the gate fidelity are derived in the limit of weak noise, which covers the regime of experimental parameters [6, 8, 25]. We also quantify the effect of charge noise by two-qubit randomized benchmarking (RB), and the results suggest that the noise averaged sequential fidelity still decays according to an exponential-law at the realistic noise strength.

This paper is organized as follows. In Sec. II, we introduce the model for the DQD system, together with the quasistatic description for the charge noise. Meanwhile, the average effect on the model Hamiltonian is also derived. In Sec. III, the implementation of the CPHASE gate was discussed, with the derivation of perturbative results for the spin-up fraction and the gate fidelity. We supplied those results in Sec. IV by the two-qubit interleaved RB simulation on the CPHASE gate. Finally, we summarize and draw the conclusion in Sec. V.

\* ynfang@ynu.edu.cn

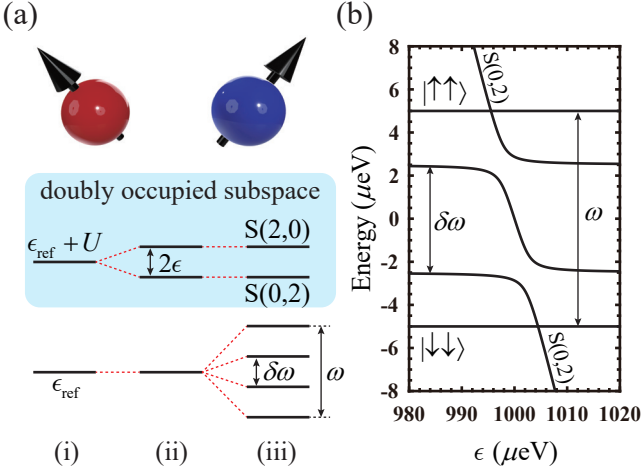


Figure 1. (a) Schematic plot of a double quantum dot (DQD) and its energy levels in the two electrons subspace. The red and blue dots are subjected to different magnetic fields along the  $z$ -direction. In the bottom panel, from left to right the accumulated effects on the level splitting are: (i) Coulomb repulsion  $U$ ; (ii) Voltage detuning  $\epsilon$ ; (iii) Zeeman splitting  $\omega$  and  $\delta\omega$  due to the inhomogeneous magnetic field.  $\epsilon_{\text{ref}}$  is a referential energy point. (b) Energy levels as a function of the voltage detuning  $\epsilon$  near the  $S(0,2)$ - $(1,1)$  anti-crossing. Parameters are chosen for a clear demonstration of the energy levels near the anti-crossing:  $\epsilon_{\text{ref}} = 0$ ,  $t = 1\mu\text{eV}$ ,  $\omega = 10\mu\text{eV}$ ,  $\delta\omega = 5\mu\text{eV}$ , and  $U = 1\text{meV}$ .

## II. THE MODEL

Our model consists of a double quantum dot (DQD) subjected to an inhomogeneous magnetic in the  $z$ -direction, see FIG. 1 (a). We describe the model with the Hubbard Hamiltonian [16],

$$\hat{H} = \sum_{\sigma \in \{\uparrow, \downarrow\}} \left[ \sum_{j=1,2} \epsilon_{j,\sigma} \hat{d}_{j,\sigma}^\dagger \hat{d}_{j,\sigma} + \left( t e^{i\phi} \hat{d}_{1,\sigma}^\dagger \hat{d}_{2,\sigma} + \text{h.c.} \right) \right] + U \sum_j \hat{n}_{j,\uparrow} \hat{n}_{j,\downarrow}, \quad (1)$$

where  $\hat{d}_{j,\sigma}$  annihilates an electron of spin  $\sigma$  on dot  $j$ , and  $\hat{n}_{j,\sigma} \equiv \hat{d}_{j,\sigma}^\dagger \hat{d}_{j,\sigma}$  is the corresponding electron number operator. The first line of Eq. (1) describes the combined effects of voltage detuning, Zeeman splitting due to magnetic field, as well as the tunneling coupling between the two dots. The second line of Eq. (1) describes the on-site Coulomb repulsion.

In order to better distinguish the detuning and magnetic fields effects that both contained in  $\epsilon_{j,\sigma}$ , one could introduce another set of parameters (setting  $\hbar \equiv 1$ ):

$$\epsilon_j = \frac{1}{2} (\epsilon_{j,\uparrow} + \epsilon_{j,\downarrow}), \quad \omega_j = \epsilon_{j,\uparrow} - \epsilon_{j,\downarrow}, \quad (2)$$

With  $\epsilon_j$  and  $\omega_j$ , the detuning of the first dot with respect

to the second dot is given by

$$\epsilon = \epsilon_1 - \epsilon_2, \quad (3)$$

while the inhomogeneous magnetic field leads to the following Zeeman energy difference between the two dots

$$\delta\omega = \omega_1 - \omega_2. \quad (4)$$

The required local magnetic field difference for  $\delta\omega$  could be generated by several methods, by micromagnet [7, 26, 27] or dynamical nuclear polarization [28], in silicon QDs by the Stark effect [6, 25], or in cross-bar architecture by external current [11]. For the convenience of analysis we also introduce the total Zeeman splitting  $\omega \equiv \omega_1 + \omega_2$ , as well as an energy referential point  $\epsilon_{\text{ref}} = \epsilon_1 + \epsilon_2$ .

The physical meaning of the above parameters can be clearly seen from the energy spectrum of  $\hat{H}$ , which is depicted in FIG. 1 under the two-electron subspace. In the absence of tunneling coupling  $t = 0$ , the quantities  $\omega$  and  $\delta\omega$  give the respective energy spacing between the spin parallel ( $|\uparrow, \uparrow\rangle$  and  $|\downarrow, \downarrow\rangle$ ) and spin anti-parallel ( $|\uparrow, \downarrow\rangle$  and  $|\downarrow, \uparrow\rangle$ ) subspaces. For realistic consideration, the reported value of  $\omega$  in the DQD based on the isotopically purified silicon is about  $160\mu\text{eV}$  [8, 25], which corresponds to a magnetic field of 1.4T. Electrically tuning of the  $g$ -factor provides a Zeeman field difference  $\delta\omega = 0.16\mu\text{eV}$  ( $\delta\omega/h = 40\text{MHz}$ ) [6, 8]. Finally, the tunneling coupling about  $4\mu\text{eV}$  was obtained from fitting the ESR spectrum to the Hubbard model, while the Coulomb repulsion  $U$  was estimated to be  $220\text{meV}$  in Ref. [29].

The separation of energy scales  $U \gg |\delta\omega|, |\omega|$  allows one to derive an effective description of the DQD. In particular, except when the detuning  $\epsilon$  was tuned close to  $\epsilon \simeq \pm U$ , states with a doubly occupied dot, i.e.,  $|S(2,0)\rangle \equiv \hat{d}_{1,\uparrow}^\dagger \hat{d}_{1,\downarrow}^\dagger |0\rangle$  or  $|S(0,2)\rangle \equiv \hat{d}_{2,\uparrow}^\dagger \hat{d}_{2,\downarrow}^\dagger |0\rangle$ , would always energetically be separated from the other four  $(1,1)$  states  $|\sigma, \sigma'\rangle$  ( $\sigma, \sigma' \in \{\uparrow, \downarrow\}$ ), thus the two doubly occupied states could be eliminated by the Schrieffer-Wolf transformation [30, 31], leading to the following effective Hamiltonian

$$\hat{H}_{\text{eff}} = \epsilon_{\text{ref}} - \frac{J_{\text{eff}}}{4} + J_{\text{eff}} \hat{\mathbf{S}}_1 \cdot \hat{\mathbf{S}}_2 + \frac{1}{2} [\omega (\hat{S}_1^z + \hat{S}_2^z) + \delta\omega' (\hat{S}_1^z - \hat{S}_2^z)]. \quad (5)$$

Here, the exchange interaction  $J_{\text{eff}}$  depends on the tunneling coupling as well as the detuning as follows [15, 16]

$$J_{\text{eff}} = t^2 \left( \frac{1}{\Omega_{\uparrow,\downarrow}} + \frac{1}{\Omega_{\downarrow,\uparrow}} \right), \quad (6)$$

where

$$\frac{1}{\Omega_{\sigma,\sigma'}} = \frac{1}{E_{S(0,2)} - E_{\sigma,\sigma'}} + \frac{1}{E_{S(2,0)} - E_{\sigma,\sigma'}}, \quad (7)$$

and  $E_j$  denotes the energy of the DQD eigenstate  $|j\rangle$  in the absence of the tunneling coupling, i.e.,

$$E_{S(2,0)} = 2\epsilon_1 + U, \quad E_{S(0,2)} = 2\epsilon_2 + U, \quad (8)$$

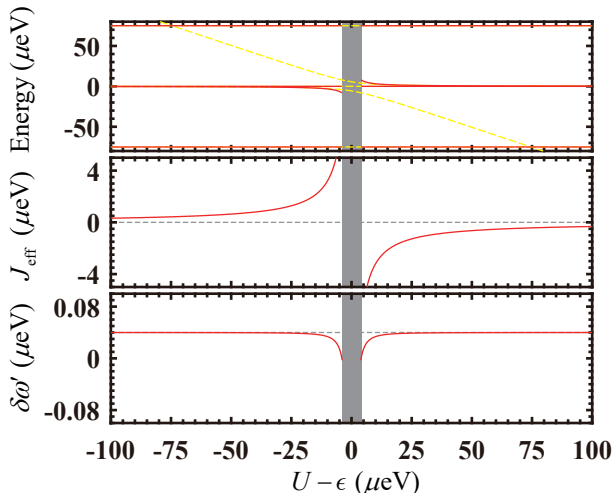


Figure 2. Energy spectrum and parameters from the effective Hamiltonian  $\hat{H}_{\text{eff}}$  in Eq. (5) near the S(0,2)-(1,1) anti-crossing. The gray shaded region is defined by  $|U - \epsilon| \leq |t - \delta\omega/2|$ , inside this region the effective model become invalid. The red curves are solved from Eqs. (5,6,10) while the yellow dashed curves in the top panel are energies obtained from the full Hamiltonian Eq. (1). Parameters used in the calculations:  $t = 4\mu\text{eV}$ ,  $\epsilon_{\text{ref}} = 0$ ,  $\omega = 150\mu\text{eV}$ ,  $\delta\omega = 0.04\mu\text{eV}$ , and  $U = 220\text{meV}$ .

and

$$E_{\uparrow,\downarrow} = \epsilon_{\text{ref}} + \delta\omega/2, \quad E_{\downarrow,\uparrow} = \epsilon_{\text{ref}} - \delta\omega/2. \quad (9)$$

Because of the tunneling coupling, the Zeeman energy difference  $\delta\omega$  is modified to  $\delta\omega'$ , which is defined as follows

$$\delta\omega' = \delta\omega - t^2 \left( \Omega_{\uparrow,\downarrow}^{-1} - \Omega_{\downarrow,\uparrow}^{-1} \right). \quad (10)$$

In deriving Eq. (5) we have neglected the higher order terms  $\sim o(t^2\Omega_{\sigma,\sigma'}^{-2})$ , thus the effective Hamiltonian is valid only when  $\epsilon$  is at least  $|t - |\delta\omega|/2|$  away from the the S(0,2)-(1,1) anti-crossing point ( $\epsilon \equiv U$ ), this is demonstrated in FIG. 2 by plotting the  $J_{\text{eff}}$  and  $\delta\omega'$  as a function of the detuning  $\epsilon$  for typical parameters of the DQD.

To account for the charge noise affecting the DQD system, it would be useful to notice that the time-scale of the noise may span over a wide range. Therefore, if the noise fluctuates ( $\sim \mu\text{s}$ ) much slower than the gate operation time ( $\sim \text{ns}$ ), one may treat the noise as quasistatic [22, 24, 32]. The effect of the noise in this quasistatic limit had been modeled by assuming a Gaussian distribution for the detuning  $\epsilon$  [21, 23, 33], i.e.,

$$p(\epsilon) = \frac{1}{\sqrt{2\pi\sigma_\epsilon^2}} \exp \left[ -\frac{(\epsilon - \bar{\epsilon})^2}{2\sigma_\epsilon^2} \right], \quad (11)$$

where  $\bar{\epsilon}$  represents the average value of the detuning and the standard deviation  $\sigma_\epsilon$  quantifies the noise. The value

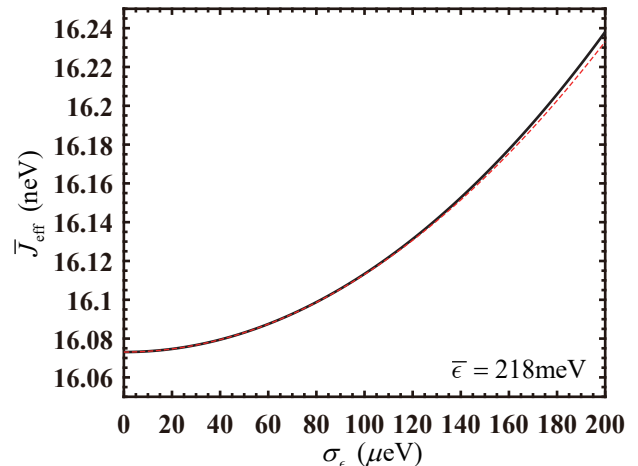


Figure 3. Average exchange interaction  $\bar{J}_{\text{eff}}$  as a function of the standard deviation  $\sigma_\epsilon$  of the distribution  $p(\epsilon)$ . Black solid curve is obtained from the numerical integration while the red dashed curve depicts the approximation Eq. (12). Parameters used in the calculation:  $t = 4\mu\text{eV}$ ,  $\omega = 150\mu\text{eV}$ ,  $\delta\omega = 0.04\mu\text{eV}$ ,  $U = 220\text{meV}$ , and  $\bar{\epsilon} = 218\text{meV}$ .

for  $\sigma_\epsilon$  could be estimated from the  $T_2^*$  measurements and for the silicon quantum dot  $\sigma_\epsilon \simeq 28\mu\text{eV}$  [29].

Under the quasistatic limit with the Gaussian distribution model Eq. (11), one can first evaluate the relevant quantities at a fixed value of  $\epsilon$ , and the effect of the noise was then obtained as an average of that quantity with respect to the distribution  $p(\epsilon)$ . For example, let us consider here the average of  $J_{\text{eff}}$ . If  $\bar{\epsilon}$  is far from the S(0,2)-(1,1) anti-crossing point compared with the width  $\sigma_\epsilon$  of the distribution  $p(\epsilon)$ , one may perform a Taylor expansion on  $J_{\text{eff}}(\epsilon)$  around  $\bar{\epsilon}$  to the quadratic order  $(\epsilon - \bar{\epsilon})^2$  and obtain the following approximated expression for the average exchange interaction

$$\bar{J}_{\text{eff}} = \int d\epsilon J_{\text{eff}}(\epsilon)p(\epsilon) \simeq J_{\text{eff}}(\bar{\epsilon}) + \frac{\sigma_\epsilon^2}{2} J_{\text{eff}}''(\bar{\epsilon}), \quad (12)$$

where  $J_{\text{eff}}''(\epsilon) = d^2 J_{\text{eff}}/d\epsilon^2$  is the second order derivative with respect to the detuning. As compared in FIG. 3, the approximated  $\bar{J}_{\text{eff}}$  given by Eq. (12) above agrees quantitatively well with the exact result provided that  $\sigma_\epsilon \ll |U - \bar{\epsilon}|$ . For another example, by using the same approximation as in Eq. (12), one can show that the effective Hamiltonian after averaging over  $p(\epsilon)$  could be written as follows

$$\bar{H}_{\text{eff}} = \hat{H}_{\text{eff}} + \delta\hat{H}_c, \quad (13)$$

with [neglecting a constant energy shift  $-\sigma_\epsilon^2 J_{\text{eff}}''(\bar{\epsilon})/8$ ]

$$\begin{aligned} \delta\hat{H}_c = & \lambda_{\uparrow,\downarrow} \left[ \hat{\mathbf{S}}_1 \cdot \hat{\mathbf{S}}_2 - \left( \hat{S}_1^z - \hat{S}_2^z \right) \right] \\ & + \lambda_{\downarrow,\uparrow} \left[ \hat{\mathbf{S}}_1 \cdot \hat{\mathbf{S}}_2 + \left( \hat{S}_1^z - \hat{S}_2^z \right) \right], \end{aligned} \quad (14)$$

where the coupling coefficients  $\lambda_{\sigma,\sigma'}$  are defined as follows

$$\lambda_{\sigma,\sigma'} = \frac{\sigma_\epsilon^2 t^2}{2} \frac{d^2 \Omega_{\sigma,\sigma'}^{-1}}{d\epsilon^2} \Big|_{\epsilon=\bar{\epsilon}}. \quad (15)$$

Thus, the effect of the charge noise may be viewed as providing a perturbation  $\delta\hat{H}_c$  on the level of model Hamiltonian. It turns out that the main effects are in the exchange interaction and the local magnetic fields.

### III. CONTROLLED PHASE GATE

Among various two-qubit gates, the two most commonly considered ones are the swap gate and the controlled phase (CPHASE) gate. Although other types of two-qubit gates such as the controlled-not gate could also be implemented with an additional driving on the conditional transition [34], the exchange interaction has been exploited for realizing the CPHASE gate [35], thus the CPHASE gate represents a good example to investigate the effect of charge noise. Depending on the values of  $J_{\text{eff}}$  and  $\delta\omega$ , the DQD system could realize both types of quantum gates [8, 36, 37]. In particular, for weak exchange interaction  $J_{\text{eff}} \ll \delta\omega$ , the eigenstates of the DQD in the spin anti-parallel subspace are hardly affected by the tunneling coupling and resemble the product states  $|\sigma, \bar{\sigma}\rangle$  ( $\bar{\sigma}$  denotes the opposite direction to  $\sigma$ ), thus the net effect of the exchange interaction was to induce an additional frequency shifts for  $|\sigma, \bar{\sigma}\rangle$  compared with the triplet states  $|\sigma, \sigma\rangle$ . Time-accumulated dynamical phase due to this frequency shift then leads to a CPHASE gate [16]:

$$\mathbf{U}_{\text{cp}} = \begin{bmatrix} 1 & 0 & 0 & 0 \\ 0 & e^{i\phi_1} & 0 & 0 \\ 0 & 0 & e^{i\phi_2} & 0 \\ 0 & 0 & 0 & 1 \end{bmatrix}, \quad (16)$$

where the basis ordering for the above matrix is  $\{|\uparrow, \uparrow\rangle, |\uparrow, \downarrow\rangle, |\downarrow, \uparrow\rangle, |\downarrow, \downarrow\rangle\}$ . For  $\phi_1 + \phi_2 = \pi$ , the CPHASE gate  $\mathbf{U}_{\text{cp}}$  is called a controlled  $\pi$ -phase gate.

Let us consider the implementation of the CPHASE gate with the non-adiabatic scheme [35], consisting of non-adiabatically pulsing the detuning from  $\epsilon_i$  to  $\epsilon_f$  and keeping the system evolving at  $\epsilon_f$  for a period of waiting time  $t_w$  (cf. inset of FIG. 4). The non-adiabatic pulsing of  $\epsilon$  requires that the time  $t_{\text{pulse}}$ , during which  $\epsilon$  changes from  $\epsilon_i$  to  $\epsilon_f$ , should satisfy  $t_{\text{pulse}} \ll J_{\text{eff}}/\delta\omega^2$  [35]. For  $J_{\text{eff}} \sim 3\text{MHz}$  and  $\delta\omega \sim 10\text{MHz}$  this amounts to require  $t_{\text{pulse}} \ll 30\text{ns}$ , which was already demonstrated in experiments, for example charge shuttling along a linear array of 9 quantum dots can be achieved in 50ns [38].

For simplification, one may rewrite the effective Hamiltonian under a rotating frame defined by the following time-dependent unitary transformation [35]

$$\hat{R}(t) = e^{-i\omega(\hat{S}_1^z + \hat{S}_2^z)t/2}, \quad (17)$$

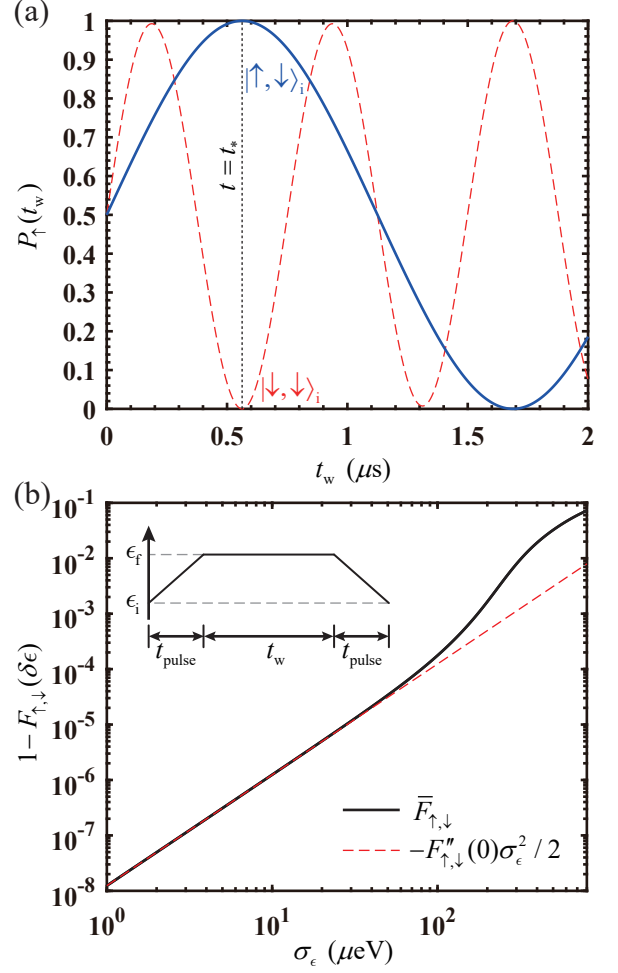


Figure 4. (a) Spin-up fraction as a function of waiting time for two different initial states. The vertical dotted line depicts  $t_w = t_*$ , where an ideal controlled phase (CPHASE) gate could be realized. (b) Gate infidelity integrated over the distribution  $p(\epsilon)$  as a function of the standard deviation  $\sigma_\epsilon$ . The black solid and red dashed curves are the exact as well as approximated results. Inset: schematic plot of the detuning as a function of time during the implementation of the CPHASE gate. Parameters used in the calculations:  $t = 4\mu\text{eV}$ ,  $\omega = 150\mu\text{eV}$ ,  $\delta\omega = 0.04\mu\text{eV}$ ,  $U = 220\text{meV}$ ,  $\epsilon_f = 218610\mu\text{eV}$ ,  $\epsilon_i = \epsilon_f - 1\text{meV}$ , and  $\bar{\epsilon} = \epsilon_f$ .

Thus the transformed effective Hamiltonian reads

$$\begin{aligned} \hat{H}_{\text{rot}} &\equiv \hat{R}^\dagger(t)\hat{H}_{\text{eff}}\hat{R}(t) - i\hat{R}^\dagger(t)\partial_t\hat{R}(t) \\ &= \epsilon_{\text{ref}} - \frac{J_{\text{eff}}}{4} + J_{\text{eff}}\hat{\mathbf{S}}_1 \cdot \hat{\mathbf{S}}_2 + \frac{\delta\omega'}{2} (\hat{S}_1^z - \hat{S}_2^z), \end{aligned} \quad (18)$$

Notice that Eq. (18) could be diagonalized with a unitary transformation via  $\hat{H}_{\text{rot}} = \hat{U}_{\text{rot}}(\epsilon)\hat{E}_{\text{rot}}\hat{U}_{\text{rot}}(\epsilon)^\dagger$ , where  $\hat{E}_{\text{rot}}$  is a diagonal matrix with diagonal elements the energies in the ascending order. By introducing Pauli matrices defined on the spin parallel (P) as well as spin

anti-parallel (AP) subspaces:

$$\hat{\tau}_P^0 = \sum_{\sigma \in \{\uparrow, \downarrow\}} |\sigma, \sigma\rangle \langle \sigma, \sigma|, \quad (19)$$

$$\hat{\tau}_{AP}^x = |\uparrow, \downarrow\rangle \langle \downarrow, \uparrow| + |\downarrow, \uparrow\rangle \langle \uparrow, \downarrow|, \quad (20)$$

$$\hat{\tau}_{AP}^z = |\uparrow, \downarrow\rangle \langle \uparrow, \downarrow| - |\downarrow, \uparrow\rangle \langle \downarrow, \uparrow|, \quad (21)$$

then

$$\hat{U}_{\text{rot}}(\epsilon) = \hat{\tau}_P^0 + \cos \frac{\theta(\epsilon)}{2} \hat{\tau}_{AP}^x - \sin \frac{\theta(\epsilon)}{2} \hat{\tau}_{AP}^z, \quad (22)$$

where the mixing angle  $\theta(\epsilon) = \arctan J_{\text{eff}}/\delta\omega'$ . Notice that the unitary transformation  $\hat{U}_{\text{rot}}(\epsilon)$  defined above is also Hermitian.

Since the system was initialized and readout at the detuning  $\epsilon_i$ , the natural basis for the discussion would be the eigenstates of  $\hat{H}_{\text{rot}}(\epsilon_i)$ . Notice that the tunneling coupling  $t$  would have much less effect on those eigenstates at the initial detuning  $\epsilon_i$  that is usually away from the  $S(0, 2)$ - $(1, 1)$  anti-crossing point, if  $|t|^2/(U|\delta\omega|) \ll 1$  [16]. In fact, one can show that to leading order of this small parameter,  $\sin \theta_i \simeq 4|t|/|\delta\omega| \cdot |t|/U$ . Thus the eigenstates in the spin anti-parallel subspace at the initial detuning would be very close to the the product basis  $|\sigma, \bar{\sigma}\rangle$ , e.g.,  $|\uparrow, \downarrow\rangle + 2|t|^2/(|\delta\omega|U) |\downarrow, \uparrow\rangle \simeq |\uparrow, \downarrow\rangle$ . Therefore, we also denote the eigenbasis at  $\epsilon_i$  using the same notation  $|\sigma, \sigma'\rangle_i$  except with a subscript  $i$  indicating  $\epsilon_i$ . By this notation we introduced the basis  $|\uparrow, \uparrow\rangle_i, |\downarrow, \uparrow\rangle_i, |\uparrow, \downarrow\rangle_i, |\downarrow, \downarrow\rangle_i$ , hereafter we refer this basis as the  $i$ -basis.

The corresponding time-evolution operator when the system was biased to  $\epsilon_f$  is written as follows

$$\begin{aligned} \hat{U}(\epsilon_f, t_w) &= e^{-i\hat{H}_{\text{rot}}(\epsilon_f)t_w} \\ &= \hat{U}_{\text{rot}}(\epsilon_f) e^{-i\hat{E}_{\text{rot}}(\epsilon_f)t_w} \hat{U}_{\text{rot}}(\epsilon_f)^\dagger \\ &= \begin{bmatrix} 1 & 0 & 0 & 0 \\ 0 & \cos^2 \frac{\theta_i - \theta_f}{2} e^{-i\varphi_-} + \sin^2 \frac{\theta_i - \theta_f}{2} e^{-i\varphi_+} & \frac{\sin(\theta_i - \theta_f)}{2} (e^{-i\varphi_-} - e^{-i\varphi_+}) & 0 \\ 0 & \frac{\sin(\theta_i - \theta_f)}{2} (e^{-i\varphi_-} - e^{-i\varphi_+}) & \sin^2 \frac{\theta_i - \theta_f}{2} e^{-i\varphi_-} + \cos^2 \frac{\theta_i - \theta_f}{2} e^{-i\varphi_+} & 0 \\ 0 & 0 & 0 & 1 \end{bmatrix}. \end{aligned} \quad (23)$$

where in the last line the matrix was written under the  $i$ -basis defined above, the mixing angle  $\theta_{i/f} = \theta(\epsilon_{i/f})$  and the time-accumulated dynamical phases are

$$\varphi_{\pm} = \frac{1}{2} \left[ \pm \sqrt{\delta\omega'(\epsilon_f)^2 + J_{\text{eff}}(\epsilon_f)^2} - J_{\text{eff}}(\epsilon_f) \right] t_w. \quad (24)$$

In order to realize the ideal CPHASE gate, one would require the waiting time  $t_w$  to satisfy  $\varphi_+ = \varphi_- + 2n\pi$  with  $n$  an integer. For  $n = 1$  this yields the following condition

$$t_w = t_* \equiv \frac{2\pi}{\sqrt{\delta\omega'(\epsilon_f)^2 + J_{\text{eff}}(\epsilon_f)^2}}. \quad (25)$$

When  $t_w = t_*$ , the evolution matrix Eq. (23) becomes diagonal under the  $i$ -basis,

$$\hat{U}(\epsilon_f) = \hat{\tau}_{P,i}^0 - e^{i\pi \sin \theta_f} \hat{\tau}_{AP,i}^0, \quad (26)$$

where  $\hat{\tau}_{A,i}^0$  and  $\hat{\tau}_{AP,i}^0$  in Eq. (26) denote the identity Pauli matrix defined with respect to the  $i$ -basis. Notice that the mixing angle  $\theta_f$  depends on the detuning  $\epsilon_f$ , thus if  $\epsilon_f$  is chosen to be  $\epsilon_*$  such that  $\theta_f = \pi/6$ , then Eq. (26) realizes the inverse of  $\hat{U}_{\text{cp}}$  defined in Eq. (16) with  $\phi_1 = \phi_2 = \pi/2$ . We verified the implementation of the

CPHASE gate by calculating the spin-up fraction of the second quantum dot [25]

$$P_{\uparrow}(t_w) = \sum_{s \in \{\uparrow, \downarrow\}} |{}_i\langle s, \uparrow | \tilde{R}_y^{(2)}(\frac{\pi}{2}) \hat{U}(\epsilon_*, t_w) \tilde{R}_x^{(2)}(\frac{\pi}{2}) |\psi_0\rangle|^2, \quad (27)$$

where  $\hat{R}_\alpha^{(j)}(\theta) = \exp[-i\hat{S}_j^\alpha \theta]$  is the rotation operator for the  $j$ -th quantum dot with rotation angle  $\theta$  and rotation axis along the  $\alpha$ -direction, and  $\tilde{O} = \hat{U}_{\text{rot}}(\epsilon_i) \hat{O} \hat{U}_{\text{rot}}^\dagger(\epsilon_i)$  thus  $\tilde{R}_\alpha^{(j)}(\theta)$  is the corresponding rotation operator with spin orientation defined according to the  $i$ -basis. The results are shown in FIG. 4(a). In particular, when the waiting time  $t_w$  is chosen as  $t_*$ , the time evolution following initial state  $|\uparrow, \downarrow\rangle_i$  and  $|\downarrow, \downarrow\rangle_i$  leads to opposite behavior in  $P_{\uparrow}$ , consistent with previous studies [25].

The noise on  $\epsilon$  bias the detuning from the ideal value  $\epsilon_f^{\text{ideal}} = \epsilon_*$  such that  $\theta_f = \pi/6$  to  $\epsilon_f^{\text{actual}} = \epsilon_* + \delta\epsilon$ , which leads to errors in implementing the CPHASE gate. To quantify this error we calculated the Uhlmann fidelity between the state  $\hat{U}(\epsilon_*) |\uparrow, \downarrow\rangle_i$  and  $\hat{U}(\epsilon_* + \delta\epsilon) |\uparrow, \downarrow\rangle_i$ , which can be regarded as a gate fidelity [39], the result is given by

$$F_{\uparrow, \downarrow}(\delta\epsilon) = \cos^2 \frac{\delta\varphi}{2} + \cos^2 \delta\theta \sin^2 \frac{\delta\varphi}{2}, \quad (28)$$

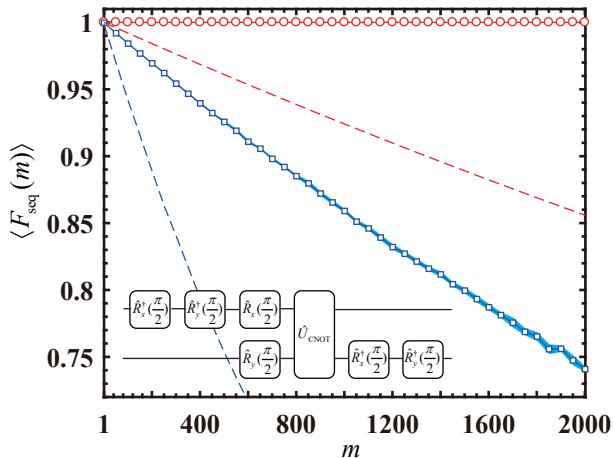


Figure 5. Two-qubit randomized benchmarking of the controlled phase gate (CPHASE) subject to an error in detuning  $\delta\epsilon_f = \epsilon_f^{\text{actual}} - \epsilon_f^{\text{ideal}}$ . Red circles (blue squares) show the averaged sequential fidelity following the standard (interleaved) RB. The blue shaded region shows the standard deviation for the interleaved RB simulation. The dashed curves show the corresponding RB simulation including a gate-independent dephasing effect. Inset: Decomposition of CPHASE gates in terms of Clifford gates, the gates on the left act first while the first (second) line represents the control (target) qubit. Parameters used in calculation:  $t = 4\mu\text{eV}$ ,  $\epsilon_{\text{ref}} = 0$ ,  $\omega = 150\mu\text{eV}$ ,  $\delta\omega = 0.04\mu\text{eV}$ ,  $U = 220\text{meV}$ ,  $1 - p_{\text{dp}} = 10^{-4}$ ,  $\delta\epsilon = 28\mu\text{eV}$ , and  $K = 500$ .

where

$$\delta\varphi = \varphi_+(\epsilon_* + \delta\epsilon) - \varphi_-(\epsilon_* + \delta\epsilon), \quad (29)$$

$$\delta\theta = \theta(\epsilon_*) - \theta(\epsilon_* + \delta\epsilon). \quad (30)$$

The corresponding gate infidelity  $1 - F_{\uparrow,\downarrow}$  averaged over the distribution  $p(\epsilon)$  with  $\bar{\epsilon} = \epsilon_*$  is shown in FIG. 4(b), for small value of  $\sigma_\epsilon$  the infidelity can be well described by the second order derivative of  $F_{\uparrow,\downarrow}$ , i.e.,  $F_{\uparrow,\downarrow}(0) + F_{\uparrow,\downarrow}''(0)\sigma_\epsilon^2/2$ . The  $\sigma_\epsilon^2$  scaling at weak noise, i.e., small  $\sigma_\epsilon$ , is a result of the Gaussian distribution that assumed for  $p(\epsilon)$ . While the deviation from  $\sigma_\epsilon^2$  scaling for a stronger noise is due to the failure of second order perturbative expansion on  $F_{\uparrow,\downarrow}$ .

#### IV. RANDOMIZED BENCHMARKING

Instead of the gate fidelity  $F_{\uparrow,\downarrow}$ , a more robust and systematic way of characterizing the noise effect on the CPHASE gate is through the interleaved randomized benchmarking (IRB) [39–43]. Usually, in a randomized benchmarking (RB) test on an  $n$ -qubits system, a sequence of  $m$  quantum gates are sampled randomly from the  $n$ -qubits Clifford group  $\mathcal{C}_n$ . The system is then

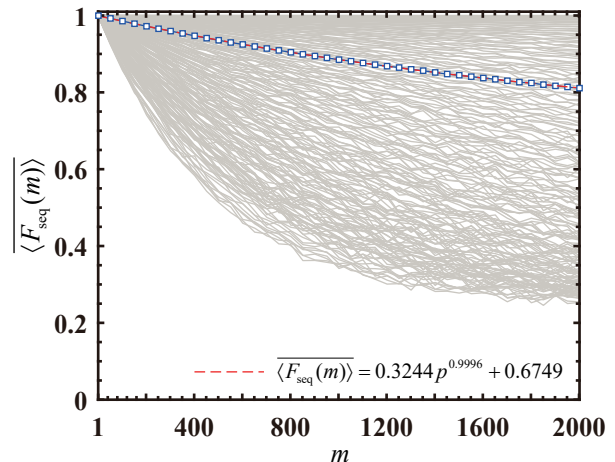


Figure 6. The sequential fidelity averaged over the charge noise distribution  $p(\epsilon)$ . The blue squares are the numerical data point while the red dashed curve is the fit to the zero-th order RB model. The gray curves represents 200 RB simulations with different detuning errors  $\delta\epsilon$  sampled uniformly within  $\epsilon_* \pm 3\sigma_\epsilon$ . Parameters used in the calculations:  $t = 4\mu\text{eV}$ ,  $\epsilon_{\text{ref}} = 0$ ,  $\omega = 150\mu\text{eV}$ ,  $\delta\omega = 0.04\mu\text{eV}$ ,  $U = 220\text{meV}$ ,  $\sigma_\epsilon = 28\mu\text{eV}$ , and  $K = 500$ .

evolved by first subjecting to the  $m$  gates then applied with a recovery gate, which in the ideal noiseless case would return the system to its initial state. Thus the wave function overlapping between the ideal and actually evolved final state provides a measure on the fidelity loss due to the noise.

The wave function overlapping is formally defined through the sequential fidelity  $F_{\text{seq}}(m)$ , given by

$$F_{\text{seq}}(m) = \text{Tr} \left\{ \hat{E}_\xi \left[ \prod_{i=1}^{m+1} \Lambda_i \circ \mathcal{C}_i \right] \hat{\rho}_0 \right\}, \quad (31)$$

Here,  $\{\hat{E}_\xi\}$  is a set of measurement operators with possible outcomes  $\{\xi\}$ , the complete positive and trace-preserving (CPTP) quantum operation  $\Lambda_i$  describes the noisy effects including decoherence during the implementation of Clifford gate  $\mathcal{C}_i$ , while  $\hat{\rho}_0$  is the initial state of the benchmarked quantum system.

Here we consider the randomized benchmarking (RB) based on the Clifford gates, the ideal CPHASE gate Eq. (16) with  $\phi_1 = \phi_2 = \pi/2$  can be decomposed in terms of two-qubit Clifford gates as shown in FIG. 5 in the sense of having identical Pauli transfer matrices. In FIG. 5 we show the (SRB) standard as well as (IRB) interleaved RB simulation results under a fixed detuning error  $\delta\epsilon = 28\mu\text{eV}$ . The IRB simulation assuming an additional gate-independent dephasing process with  $\Lambda[\hat{\rho}] = p_{\text{dp}}\hat{\rho} + 2(1 - p_{\text{dp}})\sum_{i=1,2}\hat{S}_i^z\hat{\rho}\hat{S}_i^z$  and  $1 - p_{\text{dp}} = 10^{-4}$  was also shown. Fitting the IRB data to the zero-th order fitting model [41]

$$\langle F_{\text{seq}}(m) \rangle = Ap^m + B, \quad (32)$$

gives  $p = 0.9998$ , where the bracket  $\langle F_{\text{seq}}(m) \rangle$  means to average  $F_{\text{seq}}(m)$  over the random sequences of gates with length  $m$ . Thus the gate error associated with the CPHASE gate was extracted to be  $1.5 \times 10^{-4}$ , which is slightly larger than the  $10^{-5}$  infidelity estimated from the spin-up fraction calculation.

The effect of charge noise on the RB simulation can be obtained by further averaging  $\langle F_{\text{seq}}(m) \rangle$  over the distribution  $p(\epsilon)$  with  $\bar{\epsilon} = \epsilon_*$ , i.e.,

$$\overline{\langle F_{\text{seq}}(m) \rangle} = \int d\epsilon p(\epsilon) \langle F_{\text{seq}}(m) \rangle, \quad (33)$$

The resulting decaying behavior of  $\overline{\langle F_{\text{seq}}(m) \rangle}$  is shown in FIG. 6 for  $\sigma_\epsilon = 28\mu\text{eV}$ . It turns out that the zero-th order fitting model Eq. (32) still provides quantitative well fit to the simulated data for the realistic parameters used in this study. However, we notice that in general  $\overline{\langle F_{\text{seq}}(m) \rangle}$  may deviates from the exponential decay behavior predicted by Eq. (32), e.g., power-law decay of the sequential fidelity had been reported in previous studies for single qubit due to the noise in qubit frequency [44].

In the RB simulation we have focused on the the reported realistic parameters and did not considered the full parameter space. Clearly, as suggested from the gate fidelity calculation in Sec. III, as long as  $\sigma_\epsilon$  becomes larger enough one may expect the deviation from the approximation  $F_{\uparrow,\downarrow}(0) + F_{\uparrow,\downarrow}'(0)\sigma_\epsilon^2/2$ . Also, in the simulation here we have neglected the effect of decoherence and focused on the influence of control errors related to the detuning, thus the sequential fidelity decays much slower

than those found in experiments. As can be seen in FIG. 5, inclusion of pure dephasing on the qubit could leads to fast decay of the sequential fidelity, which is qualitatively consistent with recent experiment on isotopically purified silicon system, where the sequential fidelity on a controlled rotation gate already decays for a sequence with 60 gates [8].

## V. CONCLUSION

In this work, we have explored the effect of charge noise on the controlled phase gate in a double quantum dot. By assuming quasistatic noise on the dot detuning, we have derived simple expressions for the Hamiltonian, the exchange interaction, as well as the gate fidelity that are valid under weak noise relevant for experiments. Those analyses were also supplied with the randomized benchmarking simulations, showing that an exponential decay of the sequential fidelity could be still valid under noise average. Those results would be helpful for a better understanding of charge noise effect and the design of high fidelity two-qubit gates in semiconductor based spin qubits.

## ACKNOWLEDGMENTS

The author thanks Stefano Chesi for very helpful discussions. Y.F. acknowledges support from NSFC (Grant No. 12005011) and Yunnan Fundamental Research Projects (Grant No. 202201AU070118).

- 
- [1] D. Loss and D. P. DiVincenzo, Phys. Rev. A **57**, 120 (1998).
  - [2] R. Hanson, L. P. Kouwenhoven, J. R. Petta, S. Tarucha, and L. M. K. Vandersypen, Rev. Mod. Phys. **79**, 1217 (2007).
  - [3] S. B. Bravyi and A. Y. Kitaev, arXiv: quant-ph/9811052.
  - [4] E. Dennis, A. Y. Kitaev, A. Landahl, and J. Preskill, J. Math. Phys. **43** (2002).
  - [5] A. Fowler, M. Mariantoni, J. M. Martinis, and A. N. Cleland, Phys. Rev. A **86** (2012).
  - [6] M. Veldhorst, J. C. C. Hwang, C. H. Yang, A. W. Leenstra, B. de Ronde, J. P. Dehollain, J. T. Muhonen, F. E. Hudson, K. M. Itoh, A. Morello, and A. S. Dzurak, Nat. Nanotechnol. **9**, 981 (2014).
  - [7] J. Yoneda, K. Takeda, T. Otsuka, T. Nakajima, M. R. Delbecq, G. Allison, T. Honda, T. Koder, S. Oda, Y. Hoshi, N. Usami, K. M. Itoh, and S. Tarucha, Nat. Nanotechnol. **13**, 102 (2018).
  - [8] W. Huang, C. H. Yang, K. W. Chan, T. Tanttu, B. Hensen, R. C. C. Leon, M. A. Fogarty, J. C. C. Hwang, F. E. Hudson, K. M. Itoh, A. Morello, A. Laucht, and A. S. Dzurak, Nature **569**, 532 (2019).
  - [9] D. Hill Charles, P. Eldad, J. Hile Samuel, G. House Matthew, F. Martin, R. Sven, Y. Simons Michelle, and L. Hollenberg Lloyd C., Sci. Adv. **1**, e1500707 (2015).
  - [10] M. Veldhorst, H. G. J. Eenink, C. H. Yang, and A. S. Dzurak, Nat. Commun. **8**, 1766 (2017).
  - [11] R. Li, L. Petit, D. P. Franke, J. P. Dehollain, J. Helsen, M. Steudtner, N. K. Thomas, Z. R. Yoscovits, K. J. Singh, S. Wehner, L. M. K. Vandersypen, J. S. Clarke, and M. Veldhorst, Sci. Adv. **4**, eaar3960 (2018).
  - [12] M. Tadokoro, T. Nakajima, T. Kobayashi, K. Takeda, A. Noiri, K. Tomari, J. Yoneda, S. Tarucha, and T. Koder, Sci. Rep. **11**, 19406 (2021).
  - [13] P.-A. Mortemousque, E. Chanrion, B. Jadot, H. Flentje, A. Ludwig, A. D. Wieck, M. Urdampilleta, C. Bauerle, and T. Meunier, Nat. Nanotechnol. **16**, 296 (2021).
  - [14] L. Petit, M. Russ, G. H. G. J. Eenink, W. I. L. Lawrie, J. S. Clarke, L. M. K. Vandersypen, and M. Veldhorst, Commun. Mater. **3**, 82 (2022).
  - [15] G. Burkard, Phys. Rev. B **60**, 11404 (1999).
  - [16] T. Meunier, V. E. Calado, and L. M. K. Vandersypen, Phys. Rev. B **83**, 121403 (2011).
  - [17] X. Hu and S. Das Sarma, Phys. Rev. Lett. **96**, 100501 (2006).
  - [18] M. Urdampilleta, D. J. Niegemann, E. Chanrion, B. Jadot, C. Spence, P.-A. Mortemousque, C. Bauerle, L. Hutin, B. Bertrand, S. Barraud, R. Maurand, M. Sanquer, X. Jehl, S. De Franceschi, M. Vinet, and T. Meunier, Nat. Nanotechnol. **14**, 737 (2019).

- [19] E. Chanrion, D. J. Niegemann, B. Bertrand, C. Spence, B. Jadot, J. Li, P.-A. Mortemousque, L. Hutin, R. Maurand, X. Jehl, M. Sanquer, S. D. Franceschi, C. Bauerle, F. Balestro, Y.-M. Niquet, M. Vinet, T. Meunier, and M. Urdampilleta, *Phys. Rev. Appl.* **14** (2020).
- [20] O. E. Dial, M. D. Shulman, S. P. Harvey, H. Bluhm, V. Umansky, and A. Yacoby, *Phys. Rev. Lett.* **110**, 146804 (2013).
- [21] R. E. Throckmorton, E. Barnes, and S. Das Sarma, *Phys. Rev. B* **95**, 085405 (2017).
- [22] D. Buterakos and S. Das Sarma, *Phys. Rev. B* **103**, 205402 (2021).
- [23] D. Keith, S. K. Gorman, Y. He, L. Kranz, and M. Y. Simmons, *npj Quantum Inf.* **8**, 17 (2022).
- [24] R. E. Throckmorton and S. Das Sarma, *Phys. Rev. B* **105**, 245413 (2022).
- [25] M. Veldhorst, C. H. Yang, J. C. C. Hwang, W. Huang, J. P. Dehollain, J. T. Muhonen, S. Simmons, A. Laucht, F. E. Hudson, K. M. Itoh, A. Morello, and A. S. Dzurak, *Nature* **526**, 410 (2015).
- [26] Y. Tokura, W. G. van der Wiel, T. Obata, and S. Tarucha, *Phys. Rev. Lett.* **96**, 047202 (2006).
- [27] S. Chesi, Y.-D. Wang, J. Yoneda, T. Otsuka, S. Tarucha, and D. Loss, *Phys. Rev. B* **90**, 235311 (2014).
- [28] R. Thalineau, S. R. Valentin, A. D. Wieck, C. Bäuerle, and T. Meunier, *Phys. Rev. B* **90**, 075436 (2014).
- [29] U. Güngördü and J. P. Kestner, *Phys. Rev. B* **98**, 165301 (2018).
- [30] J. R. Schrieffer, *Theory of Superconductivity* (W. A. Benjamin and Company, Inc., New York, 1964).
- [31] J. R. Schrieffer and P. A. Wolff, *Phys. Rev.* **149**, 491 (1966).
- [32] E. Ferraro, M. Fanciulli, and M. De Michielis, *J. Phys. Commun.* **2**, 115022 (2018).
- [33] Y. He, S. K. Gorman, D. Keith, L. Kranz, J. G. Keizer, and M. Y. Simmons, *Nature* **571**, 371 (2019).
- [34] I. Heinz and G. Burkard, *Phys. Rev. B* **104**, 045420 (2021).
- [35] M. Russ, D. M. Zajac, A. J. Sigillito, F. Borjans, J. M. Taylor, J. R. Petta, and G. Burkard, *Phys. Rev. B* **97**, 085421 (2018).
- [36] M. Veldhorst, R. Ruskov, C. H. Yang, J. C. C. Hwang, F. E. Hudson, M. E. Flatté, C. Tahan, K. M. Itoh, A. Morello, and A. S. Dzurak, *Phys. Rev. B* **92**, 201401 (2015).
- [37] T. F. Watson, S. G. J. Philips, E. Kawakami, D. R. Ward, P. Scarlino, M. Veldhorst, D. E. Savage, M. G. Lagally, M. Friesen, S. N. Coppersmith, M. A. Eriksson, and L. M. K. Vandersypen, *Nature* **555**, 633 (2018).
- [38] A. R. Mills, D. M. Zajac, M. J. Gullans, F. J. Schupp, T. M. Hazard, and J. R. Petta, *Nat. Commun.* **10**, 1063 (2019).
- [39] E. Magesan, J. M. Gambetta, and J. Emerson, *Phys. Rev. A* **85**, 042311 (2012).
- [40] J. Emerson, R. Alicki, and K. Zyczkowski, *J. Phys. B At. Mol. Opt.* **7**, s347 (2005).
- [41] E. Magesan, J. M. Gambetta, B. R. Johnson, C. A. Ryan, J. M. Chow, S. T. Merkel, M. P. da Silva, G. A. Keefe, M. B. Rothwell, T. A. Ohki, M. B. Ketchen, and M. Steffen, *Phys. Rev. Lett.* **109**, 080505 (2012).
- [42] J. J. Wallman and S. T. Flammia, *New J. Phys.* **16**, 103032 (2014).
- [43] J. M. Epstein, A. W. Cross, E. Magesan, and J. M. Gambetta, *Phys. Rev. A* **89**, 062321 (2014).
- [44] M. A. Fogarty, M. Veldhorst, R. Harper, C. H. Yang, S. D. Bartlett, S. T. Flammia, and A. S. Dzurak, *Phys. Rev. B* **92**, 022326 (2015).